ISSN 0915-633X

NATIONAL INSTITUTE FOR FUSION SCIENCE

Effects of Net Toroidal Current Profile on Mercier Criterion in Heliotron Plasma

K. Ichiguchi, T. Nishimura, N. Nakajima, M. Okamoto,
S.-i. Oikawa and M. Itagaki

(Received - Jan. 24, 2001)

NIFS-692 Apr. 2001

RESEARCH REPORT
NIFS Series

TOKI, JAPAN

Effects of Net Toroidal Current Profile on Mercier Criterion in Heliotron Plasma

Katsuji Ichiguchi, Takehito Nishimura[A], Noriyoshi Nakajima,
Masao Okamoto, Shun-ichi Oikawa[A], Masafumi Itagaki[A]
National Institute for Fusion Science, Toki 509-5292, Japan
Hokkaido University, Sapporo 060-8628, Japan[A]

Abstract

The effects of the variation in the net toroidal current on the Mercier criterion are studied in a Heliotron configuration under the free boundary condition. The plasma column and the magnetic axis are shifted horizontally by the net toroidal current because the effective vertical field is changed. The direction of the shift depends on the direction of the current. In the case of the subtractive current which decreases the rotational transform, the equilibrium is more stable than the no net current equilibrium, although the plasma axis is shifted inward by the current itself. This is because the Shafranov shift is superior to the axis shift by the current and the magnetic well is enhanced. In the case of the additive current which increases the rotational transform, there is a tendency that the stability is improved as the peak position of the current density varies from the axis to the peripheral region. This improvement is due to the enhancement of the magnetic shear at low beta and the magnetic well at high beta. When the subtractive current peaked at the axis and the additive hollow current flow simultaneously so that the total current should be zero or slightly additive, the interchange mode can be stabilized even if the corresponding equilibrium with no net current is strongly Mercier unstable.

Keywords: Heliotron, Mercier criterion, net toroidal current, free boundary equilibrium

Classification No. C0.St

1 Introduction

In the heliotron configurations, net toroidal current is not needed for the generation of the confinement magnetic field. However, substantial net toroidal currents over 100kA have been observed in the recent discharges in the Large Helical Device (LHD)[1], which is considered to be composed of the bootstrap current[2] and the Ohkawa current[3]. These currents have different property in the profile of the current density. The bootstrap current is induced by the thermodynamic forces driven by the gradients of the temperature and the density. Therefore, the current density is hollow and zero at the magnetic axis. On the other hand, the Ohkawa current is generated by the neutral beam injection. The profile is mainly determined by the birth profile of the energetic ions due to the charge exchanges and the ionizations by the thermal ions. Hence the profile of the current density has a tendency to be peaked at the magnetic axis for a peaked pressure profile.

The effects of the net toroidal current on the magnetohydrodynamic (MHD) stability has been studied extensively in the heliotron configurations. Recent theoretical works have revealed that such net toroidal current has a strong effect on the pressure driven mode. Ichiguchi et al.[4] investigated the effects of the current of which the current density is peaked at the magnetic axis on the Mercier criterion[5, 6] of the LHD plasma. This current density profile is close to that of the Ohkawa current. They showed that the Mercier stability depends on the direction of the peaked current, that is, the additive current which increases the rotational transform has a destabilizing contribution and the subtractive current which decreases the rotational transform has a stabilizing contribution.

To know the effects of the bootstrap current, Ichiguchi[8] calculated the bootstrap current which is self-consistent with the three-dimensional LHD equilibrium based on the neoclassical transport[9]. He assumed that both profiles of the temperature and the density are parabolic and the electron temperature equals to the ion temperature. It was shown that the substantial bootstrap current flows in the additive direction in the low collisionality regime. The obtained current density at the magnetic axis is zero, however, the profile is highly localize around the magnetic axis. In this case, the Mercier stability is remarkably deteriorated compared with the no net current case. This result is consistent with the case of the peaked current density and the mechanism of the destabilization can be explained in the same way as Ref.[4].

On the other hand, Matsumoto et al.[7] investigated the influence of the bootstrap current on the stability with a model current density. They used hollow current density profiles which are zero at the magnetic axis. They obtained that the Mercier stability is improved by the net toroidal current with hollow current density profile even in the case where the current flows in the additive direction. This result seems to be inconsistent with above results at a glance. However, there is a difference in the current density profile. They assumed the current density profile localized in the peripheral region so that the peak positions of the current density should be located for $\rho_p \geq 0.7$, while the peak position is located at $\rho_p = 0.2$ in the results of Ref.[8], where ρ is the square root of the normalized toroidal magnetic flux as the coordinate for the minor radius and ρ_p denotes the peak position in the ρ coordinate.

These results suggest that the Mercier stability is affected by not only the direction of the total net current but also the current density profile. Thus, the effects of the current density profile on the Mercier stability is studied numerically in this work. In order to understand the effects of the profile comprehensively, we investigate the equilibria with both hollow profiles and peaked profiles at the magnetic axis. Particularly, the profile of the bootstrap current should be hollow, however the peak position can be variable depending on Z_{eff}, the profiles of the temperature and the density of each particle, and the geometrical factor determined by the collisionality of the particles and the magnetic structure of the equilibrium. Therefore, as for the hollow current density profile, we examine the stability property by changing the peak position in the range of $0.2 \leq \rho_p \leq 0.7$ in the plasma column. This investigation gives the relation between the results of Refs.[4] and [7]. Furthermore, in the calculation of three-dimensional equilibria with the net currents we employ the free boundary conditions, while all the above results were studied under the fixed boundary condition. By using the free boundary condition, we can consider the stability property including the effects of the plasma column shift.

Matsumoto et al. also suggested that the Mercier stable equilibria can be improved in the case that both the additive hollow current located in the peripheral region and the subtractive current peaked at the magnetic axis flow simultaneously so that the sum of the net currents should be zero[7]. This calculation is important because it is suggested that the stability of the equilibrium should be changed by the local profile of the current

density even if the net current is zero as a total, and such combination of the currents can be achieved in experiments by the combination of the bootstrap current and the Ohkawa current. However, Matsumoto et al. only examined the case of a marginal stable equilibrium as the corresponding no net current case and a hollow current with $\rho_p = 0.7$ for the bootstrap current. Therefore, it is not clear how effective such combination of the currents is in the stabilization against the Mercier modes. Thus, we extend their study to the analysis for the profile dependence of the stability by using the unstable equilibria for the corresponding no net current case and changing the peak position of the hollow current density.

This paper is organized in the following way. The numerical condition and the magnetic configuration used in the calculation are summarized in Section 2. The free boundary effect on the equilibrium carrying the net toroidal current in the LHD configuration is discussed in Section 3. The Mercier stability properties in the change of the current density profile are shown in Section 4. In Section 5, the results of the Mercier stability in the case of the combination of the hollow and peaked currents are presented. Conclusions are given in Section 6.

2 Magnetic Configuration and Numerical condition

We calculated the three-dimensional MHD equilibria by using the VMEC code[10, 11] for the research of the effects of the net toroidal current density on the Mercier criterion. The free boundary condition is employed in the calculations to include the influence of the plasma column shift. In this case, an additional constraint is needed in the determination of the plasma boundary. We choose the constraint that the position of the most outward edge in the horizontal ellipse at finite beta value should be fixed at the position in the vacuum configuration[12]. This constraint is based on the assumption that the stochasticity of the field lines at the separatrix plays a role of a virtual limiter to limit the plasma volume.

The magnetic configuration examined here is the LHD configuration with the vacuum magnetic axis located at 3.6m and the magnetic field strength at the center of the helical coils being 2.77T. In the third campaign of the LHD experiment, the highest beta value, $\langle\beta\rangle = 2.4\%$, was obtained in this magnetic configuration[13], where $\langle\beta\rangle$ denotes the

average beta value. The position of the right hand edge of the horizontal ellipse as the virtual limiter is determined from the result of the field line trace in the vacuum configuration, which is located at $R = 4.44$m. The pressure profile is assumed as

$$P(\rho) = P_0(1-\rho^2)(1-\rho^8). \tag{1}$$

In this case, $\langle\beta\rangle$ scales as $\langle\beta\rangle \sim \beta_0/2$, where β_0 denotes the beta value at the magnetic axis.

To study the effects of the net toroidal current comprehensively, model current density profiles are used. We consider both the current density peaked at the magnetic axis and the hollow current density vanishing at the axis. The former current density profile corresponds to the Ohkawa current, which is given by

$$J_{bm1,2}(\rho) = J_0(1-\rho^2)^2. \tag{2}$$

Both the additive and subtractive directions of the current are considered for this current density, since the direction of the Ohkawa current can be controlled by the injection angle of the neutral beam. Thus, J_{bm1} and J_{bm2} are the additive and the subtractive currents with the positive and the negative values of the factor J_0, respectively. The latter current density profile corresponds to the bootstrap current. In order to investigate the influence of the change in the peak position of the profile, we examine the three kinds of the hollow current density which are written as,

$$J_{bs1}(\rho) = J_1(\sqrt{\rho}-\rho), \tag{3}$$

$$J_{bs2}(\rho) = J_2(\rho-\rho^2) \tag{4}$$

and

$$J_{bs3}(\rho) = J_3(\rho^2-\rho^4). \tag{5}$$

The bootstrap current also can flow in either direction because the sign of the geometrical factor is variable depending on the collisionality. The current flows in the additive direction in the $1/\nu$ collisionality regime, and it can flow in the subtractive direction in the plateau regime[8]. However, the total amount of the current in the plateau regime is much smaller than that in the $1/\nu$ regime. Therefore, whenever the bootstrap current is large enough to affect the stability, it should flow in the additive direction. Thus, we set all of J_1, J_2 and J_3 positive in this study.

Figure 1 shows the profiles of the current density for the same absolute value of the total current at the plasma edge. The peak positions of the hollow currents of J_{bs1}, J_{bs2} and J_{bs3} are located $\rho_p = 0.2$, 0.5 and 0.7, respectively. The profiles of the rotational transform in the equilibria with the currents at $\beta_0 = 0.01\%$ are shown in Fig.2 for the total current of $I = 100$kA.

3 Free boundary effects on the low beta equilibria with the net toroidal current

It is known that a net toroidal current brings the so-called hoop force in a torus plasma. This force makes the plasma column shift outward in the axisymmetric configurations. It is interesting to know whether such shift of the plasma can occur in the heliotron configuration. The free boundary condition with the virtual limiter constraint which is employed in the present equilibrium calculation is suitable in the investigation of such shift of the plasma column. Figure 3 shows the positions of the center of the outermost surface and the magnetic axis for the currents of J_{bm1}, J_{bm2}, J_{bs1}, J_{bs2} and J_{bs3} at $\beta_0 = 0.01\%$ with respect to the absolute value of the total current. As shown in Fig.3(a), the direction of the shift of the center of the plasma column depends on the direction of the net toroidal current. That is, the plasma column shifts outward in the case of the additive current and inward in the case of the subtractive current. The amount of the shift is almost linear to the total current but independent of the current density profile.

The mechanism of the shift can be understood by considering the change of the effective vertical field. In general, the position of the outermost surface can be shifted by controlling the vertical field in the heliotron configuration. Since the direction of the vertical field is uniform in the whole torus, the Z-component of the poloidal field B_Z increases on one side (inside or outside) of the torus in the poloidal cross section and decreases on the other side when the vertical field is varied. If we add the vertical field so that B_Z should decrease on the outer side of the torus and increase on the inner side, the ratio B_R/B_Z increases on the outer side, where B_R is the R-component of the poloidal field. Therefore, the magnetic field line traces outward in the poloidal cross section compared with the

original configuration, i.e , the magnetic surface shifts outward[14].

In the present case of the net toroidal current, the vertical field is fixed, however, the poloidal field component is changed by the net toroidal current. The additive current which increases the poloidal field component reduces the effect of the vertical field relative to the poloidal component. In the LHD configuration, the reduction of the vertical field corresponds to the decrease of B_Z in the outer region and the increase in the inner region. As a result, the plasma column shifts outward in the torus by the same mechanism as in the vertical field control. On the contrary, the net current flows in the opposite direction, the effective vertical field is increased and the inward shift occurs. Because the variation of the poloidal field of the outermost surface is determined by the total net current, the shift is almost linear to the total current and independent of the current density profile.

The magnetic axis is also shifted by the net toroidal current as shown in Fig.3(b) where the positions of the magnetic axis at $\beta_0 = 0.01\%$ are plotted as the function of the total net current. The direction of the shift in each current is the same as that of the center of the outermost surface. However, the amount of the axis shift is larger than that of the center shift. As shown in Ref.[14], the shift of the flux surface due to the additional vertical field is proportional to the inverse of the original rotational transform at the surface. In the present case, the rotational transform at the magnetic axis is smaller than that at the edge in the no net current case. Therefore, the magnetic axis is shifted by the effective vertical field due to the current more than that of the center of the outermost surface in the same direction.

On the point of the MHD equilibrium in a torus configuration, the magnetic axis can be shifted by the Pfirsch-Schlüter current, which changes the vertical field in the plasma column. However, the toroidal current under consideration itself does not affect the position of the flux surfaces in the fixed boundary because the current is the surface quantity. Since the Pfirsch-Schlüter current is negligible at $\beta_0 = 0.01\%$, the position of the magnetic axis is determined independently of the current profile once the position of the plasma boundary is determined. Thus, as shown in Fig.3(b), the shift of the magnetic axis also depends on only the total amount of the current, not the profile of the current density.

The magnetic well strongly depends on the position of the magnetic axis relative to

the center of the outermost surface. Figure 4 shows the profile of the well depth W_d at $\beta_0 = 0.01\%$, which is defined by

$$W_d = \frac{V'(0) - V'(s)}{V'(0)}, \tag{6}$$

where s denotes the normalized toroidal flux. In this figure, the positive gradient of the curve corresponds to the magnetic well and the negative gradient corresponds to the hill. In the equilibria with the additive currents, the magnetic hill is reduced compared with that in the no net current equilibrium and the profile of the well depth is almost independent of the current density profile. This is because the magnetic axis is shifted outward more than the outermost surface by the additive current. On the contrary, the magnetic hill is enhanced in the equilibria with the subtractive current because of the inward shift of the magnetic axis.

4 Effects of the Variation of the Peak Position of the Current Density Profile

The change of the magnetic structure due to the net toroidal current influences the property of the Mercier stability. Figure 5 shows the Mercier unstable regions in (ρ, β_0) plane for the no net current, J_{bm1}, J_{bm2}, J_{bs1}, J_{bs2} and J_{bs3}. The positions of the rational surfaces of $\iota = 1, 2/3$ and $1/2$ and the contour of D_I in the unstable regions are also plotted, where ι denotes the rotational transform and D_I is the Mercier quantity normalized so that the shear term should be -1/4[6, 15]. In the no net current case, there is significant unstable region in the plasma column in the low beta regime as shown in Fig.5(b). Particularly, the region in the vicinity of the magnetic axis is strongly unstable at $\beta_0 < 3\%$, where the magnetic shear is weak and the magnetic hill spreads as shown in Figs.2 and 4, respectively. As the beta value increases, however. the unstable region shrinks. The second stability region appears beyond $\beta_0 = 5.5\%$, which is much lower than that under the fixed boundary condition[4]. That is, the free boundary equilibrium with the constraint of the virtual limiter is more stable than the fixed boundary equilibrium. This is because the magnetic axis moves outward relative to the outermost surface center at finite beta due to not only

the Pfirsch-Schlüter current as in the fixed boundary case but also the property of the vacuum magnetic surfaces[12]. This large Shafranov shift results in the enhancement of the stabilizing contribution of the magnetic well

For the current density peaked at the magnetic axis, the destabilizing contribution of the magnetic hill in the subtractive current J_{bm2} is larger than that of the additive current J_{bm1} at $\beta_0 = 0.01\%$ as discussed in Section 3. In spite of the property, the Mercier stability is deteriorated for J_{bm1} and improved for J_{bm2} compared with the no net current case as shown in Fig.5 (a) and (c), respectively. This stability results can be understood in the following way. In the low beta regime, the stabilizing effect of the magnetic shear is essential. The subtractive current of J_{bm2} enhances the magnetic shear as shown in Fig.2. The Mercier mode is almost stabilized because the enhancement of the stabilizing contribution is superior to the destabilizing contribution of the magnetic hill. On the other hand, the magnetic shear is reduced in the case of the additive current of J_{bm1}. Therefore, the stabilizing contribution is not sufficient enough to stabilize the Mercier mode driven by the magnetic hill. As the beta value increases, the Shafranov shift becomes to play an important role. Figure 6 shows the Shafranov shift δ as a function of β_0, which is defined by

$$\delta = \frac{R_{ax} - R_{cnt}}{r_{av}}, \tag{7}$$

where r_{av} denotes the average minor radius of the plasma. It is known that the Shafranov shift is roughly proportional to ι^{-2}, where ι is the rotational transform. Thus, in the subtractive current of J_{bm2} case, the axis is located inward compared with that in the no net current case at $\beta_0 = 0.01\%$, however, the increase of the shift due to the finite beta exceeds that of the no net current equilibrium because of the reduction of the rotational transform. The large Shafranov shift enhances the magnetic well. As shown in Figure 7, the well depth for J_{bm2} is much larger than that for the no net current at $\beta_0 = 4\%$, which improves the Mercier stability. On the contrary, the increase of the rotational transform at the axis brings the reduction of the Shafranov shift and the well depth in the additive current case, and therefore, the Mercier stability is deteriorated. As a result, the tendency that the additive and the subtractive current have destabilizing and stabilizing contributions to the Mercier stability for the current density peaked at the axis, respectively, is similar to the result obtained in the fixed boundary case in Ref.[4].

Figure 5 (d), (e) and (f) show the Mercier unstable regions for the hollow current density of J_{bs1}, J_{bs2} and J_{bs3}, respectively. All of the currents flow in the additive direction; however, the stability property is different depending on the peak position of the the current density profile. In the case of J_{bs1} peaked at $\rho_p = 0.2$, the equilibrium is more unstable than the no net current equilibrium and the unstable region is almost the same as that for J_{bm1}. When the peak position moves up to $\rho_p = 0.5$ corresponding to J_{bs2}, the stability in the region near the magnetic axis at low beta values is slightly improved compared with the no net current case, because the absolute value of D_I is decreased inside the unstable region. In the case of J_{bs3} peaked at $\rho_p = 0.7$, the stability is much improved for $\beta_0 < 3\%$. Particularly, the maximum value of D_I is about 0.2 along the position of the surface with $\iota = 1/2$ in this case. In the comparison study of the global stability analysis of the ideal interchange mode and the absolute value of D_I, substantial growth rate of the global mode can be found for $D_I > 0.2$[16, 17]. From this point, the global mode resonant at the surface of $\iota = 1/2$, e.g. $m = 2/n = 1$ mode, may be actually stable for J_{bs3}, where m and n are the poloidal and the toroidal mode numbers, respectively. However, the peripheral region is still unstable in the high beta region of $4\% < \beta_0 < 7\%$ as well as the cases of J_{bs1} and J_{bs2}, and the $\iota = 2/3$ surface is located in the unstable region.

The improvement of the stability at low beta in the case of J_{bs3} peaked at $\rho_p = 0.7$ is attributed to the contribution of the magnetic shear. As shown in Fig.2, the magnetic shear is enhanced only in the region for $\rho < 0.1$ at $\beta_0 = 0.01\%$ in the case of J_{bs1} compared with the case of the no net current, while the shear is enhanced almost in the whole region of the plasma in the case of J_{bs3}. Therefore, the unstable region in the low beta regime is reduced as ρ_p increases from 0.2 to 0.7.

The mechanism of the destabilization in the high beta region for the hollow currents can be explained by the property of the magnetic well. As the current flows so as to increase the rotational transform the Shafranov shifts of the three hollow currents are smaller than that of the no net current case as shown in Fig.6. It is followed that the magnetic well is reduced at finite beta as shown in Fig.7 where the well depth at $\beta_0 = 4\%$ is plotted. Hence, for all of the hollow current density cases, the Mercier stability is still unstable up to $\beta_0 = 7\%$ in the peripheral region where the magnetic hill remains.

However, there is a tendency that the unstable region is also reduced at the high beta region as ρ_p increases. This tendency results from the difference of the rotational transform. The rotational transform near the magnetic axis in the case of J_{bs3} is reduced compared with that in J_{bs1}. Therefore, the Shafranov shift of J_{bs3} is larger than that of J_{bs1}, and the stabilizing contribution of the magnetic well is much enhanced for J_{bs3} than J_{bs1} at finite beta. As a result, the Mercier stability of the equilibrium with the additive current is improved as the peak position of the current density shifts from the axis to the periphery in the plasma column including the profile peaked at the axis.

5 Superposition of the hollow current and the current peaked at the magnetic axis

There is a possibility that both the bootstrap current in the additive direction and the Ohkawa current in the subtractive direction flow simultaneously. If the amount of each net current is the same, the net toroidal current observed experimentally would be zero and the equilibrium with such currents cannot be distinguished from the no net current equilibrium. In order to know how such combination of the currents in the opposite directions influences the Mercier stability, we examine the stability by utilizing the current density profiles which are used in the study of the previous section.

Figure 8 shows the current density profiles of the superpositions of the current peaked at the magnetic axis and the hollow current, $J_{bm2} + J_{bs1}$, $J_{bm2} + J_{bs2}$ and $J_{bm2} + J_{bs3}$. The net current of each direction is 100kA, and therefore, the total amount of the current at the edge is canceled out for each combination. As shown in Fig.9, the Mercier stability is remarkably improved for all cases of the combination compared with the result of the no net current in Fig.5(b). As is in the hollow current density only, the unstable region is reduced as ρ_p increases.

In these case, the component of J_{bm2} strongly influences the magnetic shear and the magnetic well. Figure 10 shows the rotational transform profiles of the combinations of the net currents at $\beta_0 = 0.01\%$. The rotational transform near the axis is reduced by the subtractive current component and the magnetic shear is enhanced compared with that

of the no net current case. The reduction of the rotational transform near the magnetic axis leads to the enhancement of the Shafranov shift. The well depth is plotted in Fig.11 (a) for $\beta_0 = 0.01\%$ and (b) $\beta_0 = 4.0\%$. Because the total current of each case is zero, the profile of the well depth at $\beta_0 = 0.01\%$ coincides with that of the no net current case as discussed in Section 2. However, the large Shafranov shift brings the enhancement of the magnetic well as the beta value increases.

The difference of the improvement of the Mercier stability in the three combinations of the net currents depends on the hollow current component. The mechanism which generates the difference is similar to that in the hollow current density only discussed in Section 4. As ρ_p increases, the reduction of the rotational transform in the vicinity of the magnetic axis is increased, and therefore, the magnetic shear and the magnetic well is enhanced. Hence, the equilibrium with $J_{bm2} + J_{bs3}$, which has the largest reduction of the rotational transform, is the most stable in the equilibria with the combined currents.

Figure 9 shows that D_I is less than 0.2 at the rational surfaces with $\iota = 1$, $2/3$ and $1/2$ in all above three cases where the total amount of the net current is zero. If we can take the line with $D_I = 0.2$ as the stability boundary for the low-n global interchange mode, the global modes with $m \leq 3$ are actually stable in the three cases. Thus, we also calculated the equilibria with the combinations of the additive hollow current of 100kA and the subtractive current peaked at the axis of 80kA. Then, the total amount of the net current is 20kA in the additive direction. Figure 12 shows the Mercier unstable region in these cases. Because the stabilizing contribution of the subtractive current component is reduced, the equilibria are more unstable than the cases in Fig.9. However, even the equilibrium with $J_{bm2}+J_{bs1}$ is still more stable than the no net current equilibrium in spite that the substantial additive net current of 20kA flows. Besides, in the case of $J_{bm2}+J_{bs3}$ D_I is less than 0.2 in the whole region. This result implies that the additive current does not necessarily destabilize the Mercier stability.

6 Conclusions

In the present study, we examined the dependence of the Mercier stability on the net current density profile in the LHD equilibria. The free boundary condition was employed

with the constraints of the virtual limiter in the three dimensional equilibrium calculation. The additive and the subtractive net currents bring the outward and the inward shifts of the plasma column through the change of the effective vertical field, respectively. However, the contribution of the shift to the Mercier stability is small compared with the Shafranov shift due to the finite beta effect.

For the current density peaked at the magnetic axis, we obtained that the same stability tendency as in the fixed boundary case. That is, the subtractive current improves the stability and the additive current deteriorates the stability. In the case of the additive hollow current density profile, however, the Mercier stability property depends on the profile of the current density. When the peak position of the profile is located at $\rho_p = 0.2$, the stability is quite deteriorated of which the property is similar to that in the current peaked at the axis. As the peak position moves to outside in the plasma column or ρ_p increases, the stability is improved in the range of $0.2 \leq \rho_p \leq 0.7$. The mechanism of the stability improvement in the hollow additive currents is different between the low and high beta regions . In the low beta region, this stability improvement is attributed to the enhancement of the magnetic shear, while the magnetic well is the dominant contribution to the stability in the high beta region. But both mechanisms results from the change in the rotational transform. At low beta, the equilibrium with $\rho_p \geq 0.5$ is more stable than the no net current equilibrium. Hence, the additive bootstrap current, which has a hollow current density profile, can improve the Mercier stability at low beta region if the peak position is localized in the peripheral region.

When the subtractive current peaked at the axis and the additive hollow current flow simultaneously so that the total current should be canceled, the Mercier stability is remarkably improved compared with the unstable no net current equilibrium. This is due to the stabilizing contribution of the subtractive current component. It is also obtained that the stability is still improved even if the sum of the currents is slightly additive. As is in the hollow current only, the equilibrium is more stable for the larger ρ_p of the hollow current density component. Such situations can be achieved in the experiments with the unbalanced tangential neutral beam injection where the subtractive Ohkawa current and the additive bootstrap current are induced. Generally speaking, it is difficult to observe the current density profile experimentally. Hence, the equilibrium with the currents with opposite directions cannot be distinguished from the no net current equilibrium. On the

other hand, in the CHS experiments, a stable plasma was obtained beyond the Mercier unstable region which was calculated based on the no net current assumption[18]. Thus, the stabilization due to the combination of the subtractive Ohkawa currents and the additive bootstrap current may be one of the candidate of the mechanism for the stable plasma in the Mercier unstable region in the CHS.

References

[1] Watanabe,K.Y., et al., in Proc. 27th EPS Conference on Controlled Fusion and Plasma Physics, 12-16 June 2000, Budapest, Hungary, 'Study of toroidal currents and MHD equilibrium in LHD experiment' (2000).

[2] Nakajima,N., Okamoto,M., J. Phys. Soc. Jpn. **61** (1992) 833.

[3] Nakajima,N., Okamoto,M., J. Phys. Soc. Jpn. **59** (1990) 3595.

[4] Ichiguchi,K., Nakajima,N., Okamoto,M., Nakamura,Y., Wakatani,M., Nucl. Fusion **33** (1993) 481.

[5] Mercier,C., Nucl. Fusion Suppl. Pt.2, (1962) 801.

[6] Johnson,J.L., Greene,J.M., Plasma Phys. **9** (1967) 611.

[7] Matsumoto,T., Nakamura,Y., Wakatani,M., Nucl. Fusion **36** (1996) 1571.

[8] Ichiguchi,K., Plasma Phys. Control. Fusion **39** (1997) 1805.

[9] Watanabe,K.Y., Nakajima,N., Okamoto,M., et al., Nucl. Fusion **35** (1995) 335.

[10] Hirshman,S.P., Whitson,J.C., Phys. Fluids **26** (1983) 3553.

[11] Hirshman,S.P., van Rij,W.I., Merkel,P., Comp. Phys. Comm. **43** (1986) 143.

[12] Ichiguchi,K., Nakajima,N., Gardner,H.J., Nucl. Fusion **36** (1996) 1157.

[13] Sakakibara,S., et al., 18th IAEA Fusion Energy Conference (Sorrento, 2000), paper EXP3/12.

[14] Miyamoto,K., *'Plasma Physics for Nuclear Fusion'* The MIT Press, 1980, P.41.

[15] Glasser.A.H., Greene.J.M., Johnson.J.L., Phys. Fluids **18** (1975) 875

[16] Nakamura.Y., Ichiguchi.K., Wakatani.M., et al., in Proc. Joint Varenna-Lausanne International Workshop on Theory and Fusion Plasmas (Bologna, 1990) 677.

[17] Fu.G.Y., Cooper.W.A., Gruber.R., et al., Phys. Fluids **B4** (1992) 1401.

[18] Okamura.S., Matsuoka.K., Nishimura.K., et al., Plasma Physics and Controlled Nuclear Fusion Research 1994, vol.1, (IAEA, Vienna, 1995)381.

Figure Captions

Fig.1 Profiles of the net toroidal current density for the same total current. Solid, dotted, dashed, dot-dashed and two dot-dashed lines show the profiles of J_{bm1}, J_{bm2}, J_{bs1}, J_{bs2} and J_{bs3}, respectively.

Fig.2 Profiles of the rotational transform at $\beta_0 = 0.01\%$. Thick solid, thin solid, dotted, dashed, dot-dashed and two dot-dashed lines show the profiles for no net current, J_{bm1}, J_{bm2}, J_{bs1}, J_{bs2} and J_{bs3}, respectively.

Fig.3 Horizontal positions of (a) the center of the outermost surface and (b) the magnetic axis at $\beta_0 = 0.01\%$ versus the absolute value of the total current. Solid, dotted, dashed, dot-dashed and two dot-dashed lines corresponds to J_{bm1}, J_{bm2}, J_{bs1}, J_{bs2} and J_{bs3}, respectively.

Fig.4 Profiles of the well depth at $\beta_0 = 0.01\%$. Thick solid, thin solid, dotted, dashed, dot-dashed and two dot-dashed lines show the profiles for no net current, J_{bm1}, J_{bm2}, J_{bs1}, J_{bs2} and J_{bs3}, respectively.

Fig.5 Mercier unstable regions for (a) J_{bm1}, (b) no net current, (c) J_{bm2}, (d) J_{bs1}, (e) J_{bs2} and (f) J_{bs3} in the (ρ, β_0) plane. The regions encircled by the thick solid lines show unstable regions. Thin solid lines in the unstable regions are the contours of the level surface of D_I which differ by $\Delta D_I = 0.1$. Dot-dashed lines show the boundary between the magnetic well and hill regions. Dashed lines indicate the positions of the rational surfaces corresponding to $\iota = 1$, $2/3$ and $1/2$ from right to left.

Fig.6 Shafranov shift versus β_0. Thick solid, thin solid, dotted, dashed, dot-dashed and two dot-dashed lines correspond to no net current, J_{bm1}, J_{bm2}, J_{bs1}, J_{bs2} and J_{bs3}, respectively.

Fig.7 Profiles of the well depth at $\beta_0 = 4.0\%$. Thick solid, thin solid, dotted, dashed, dot-dashed and two dot-dashed lines show the profiles for no net current, J_{bm1}, J_{bm2}, J_{bs1}, J_{bs2} and J_{bs3}, respectively.

Fig.8 Profiles of the current density in the superposition of the same amount of the subtractive current J_{bm2} (dashed lines) and the additive hollow current density of (a) J_{bs1} (dotted line), (b) J_{bs2} (dot-dashed line) and (c) J_{bs3} (two dot-dashed line). Solid lines show the superposed current density profiles.

Fig.9 Mercier unstable regions for (a) $J_{bm2}(100\text{kA}) + J_{bs1}(100\text{kA})$, (b) $J_{bm2}(100\text{kA}) + J_{bs2}(100\text{kA})$ and (c) $J_{bm2}(100\text{kA}) + J_{bs3}(100\text{kA})$ in the (ρ, β_0) plane. The regions encircled by the thick solid lines show unstable regions. Thin solid lines in the unstable regions are the contours of the level surface of D_I which differ by $\Delta D_I = 0.1$. Dot-dashed lines show the boundary between the magnetic well and hill regions. Dashed lines indicate the positions of the rational surfaces corresponding to $\iota = 1$, 2/3 and 1/2 from right to left.

Fig.10 Profiles of the rotational transform at $\beta_0 = 0.01\%$. Solid, dashed, dot-dashed and two dot-dashed lines show the profiles for no net current, $J_{bm2} + J_{bs1}$, $J_{bm2} + J_{bs2}$ and $J_{bm2} + J_{bs3}$, respectively.

Fig.11 Profiles of the well depth at (a) $\beta_0 = 0.01\%$ and (b) $\beta_0 = 4.0\%$. Solid, dashed, dot-dashed and two dot-dashed lines show the profiles for no net current, $J_{bm2} + J_{bs1}$, $J_{bm2} + J_{bs2}$ and $J_{bm2} + J_{bs3}$, respectively.

Fig.12 Mercier unstable regions for (a) $J_{bm2}(80\text{kA}) + J_{bs1}(100\text{kA})$, (b) $J_{bm2}(80\text{kA}) + J_{bs2}(100\text{kA})$ and (c) $J_{bm2}(80\text{kA}) + J_{bs3}(100\text{kA})$ in the (ρ, β_0) plane. The regions encircled by the thick solid lines show unstable regions. Thin solid lines in the unstable regions are the contours of the level surface of D_I which differ by $\Delta D_I = 0.1$. Dot-dashed lines show the boundary between the magnetic well and hill regions. Dashed lines indicate the positions of the rational surfaces corresponding to $\iota = 1$, 2/3 and 1/2 from right to left.

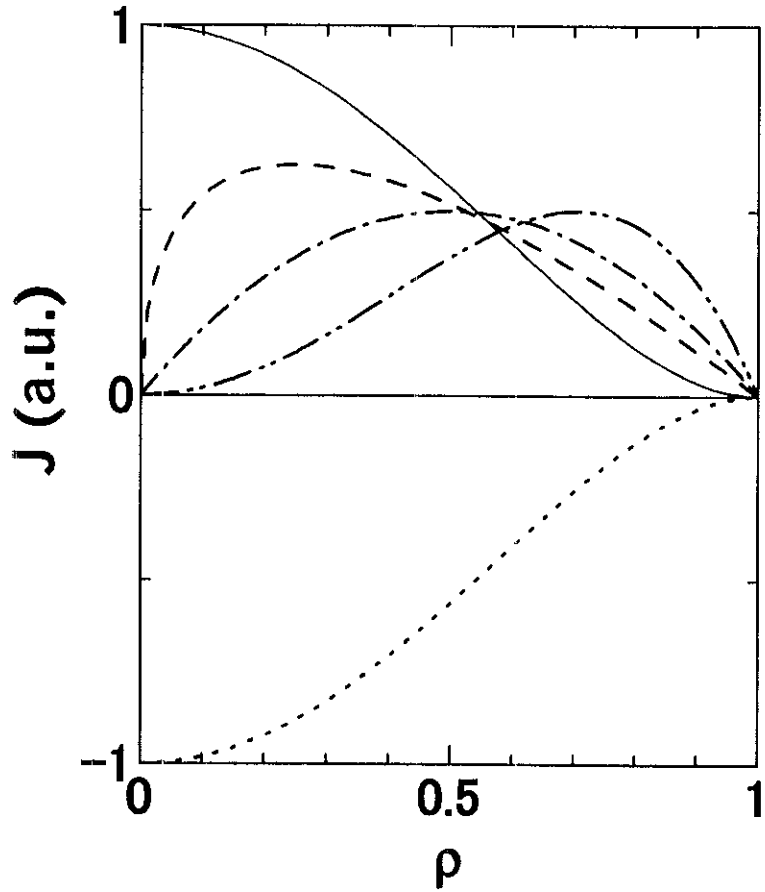

Fig.1

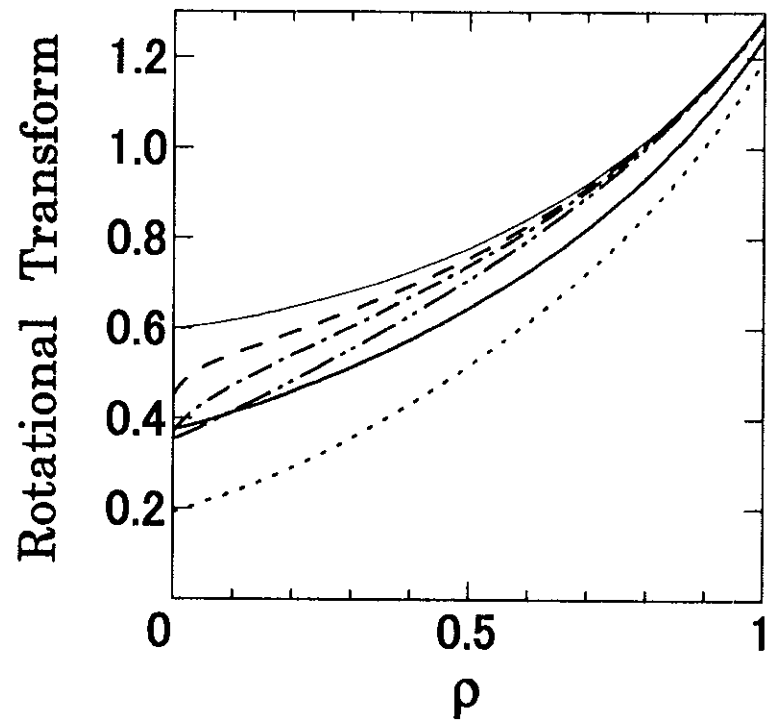

Fig.2

(a)

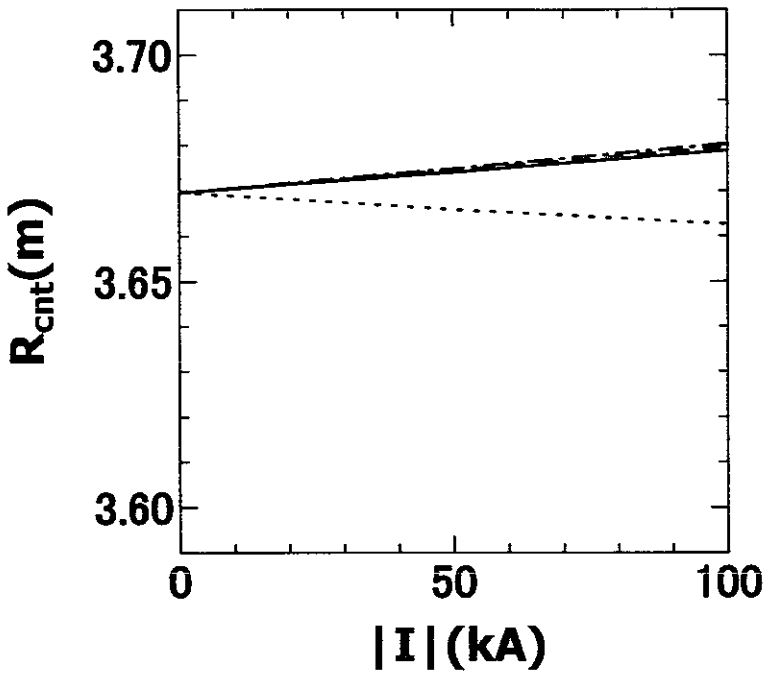

(b)

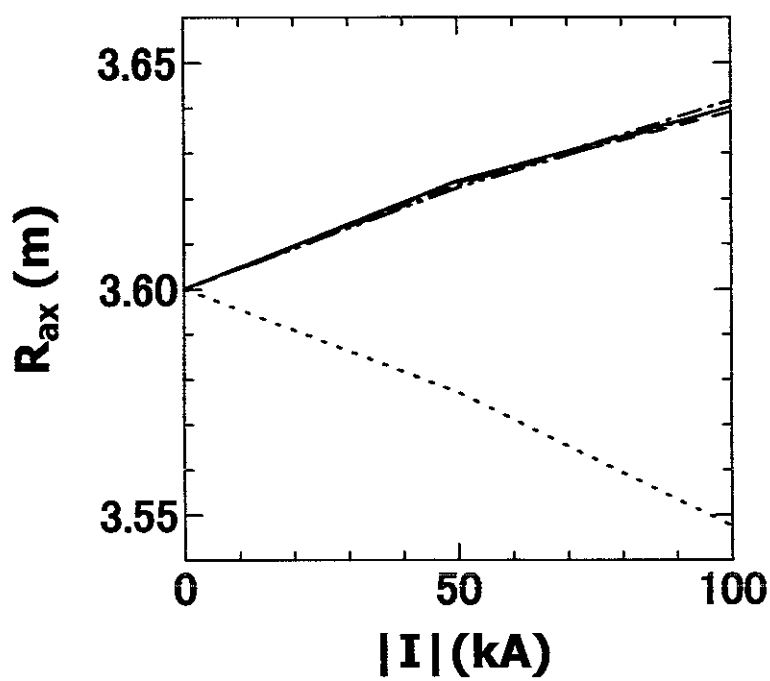

Fig.3

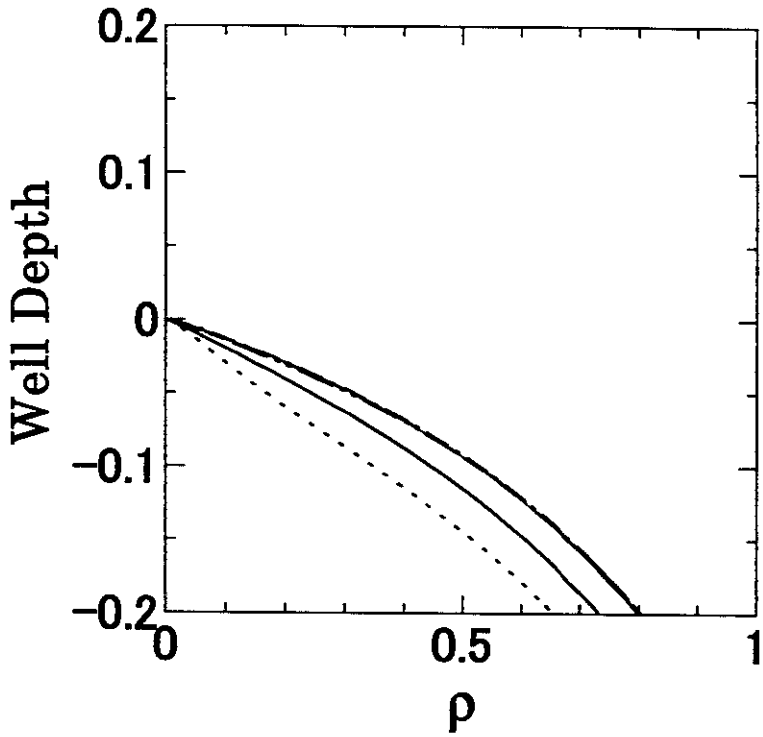

Fig.4

(a)

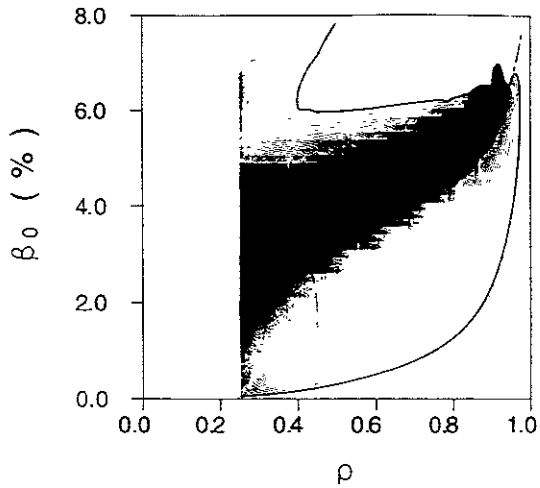
8.0
6.0
4.0
2.0
0.0
β_0 (%)
0.0
0.2
0.4
0.6
0.8
1.0
ρ

(b)

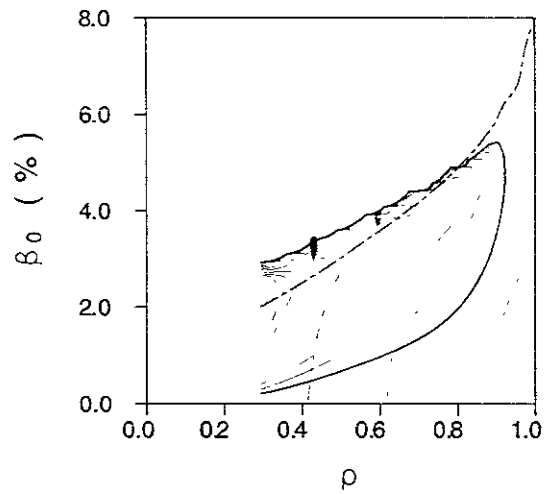
8.0
6.0
4.0
2.0
0.0
β_0 (%)
0.0
0.2
0.4
0.6
0.8
1.0
ρ

(c)

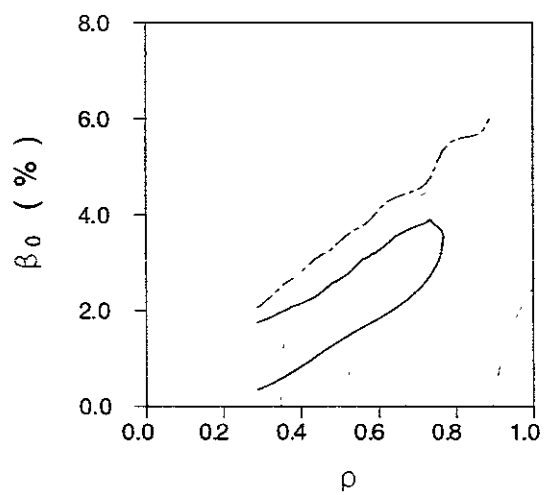
8.0
6.0
4.0
2.0
0.0
β_0 (%)
0.0
0.2
0.4
0.6
0.8
1.0
ρ

Fig.5 (a),(b),(c)

(d)

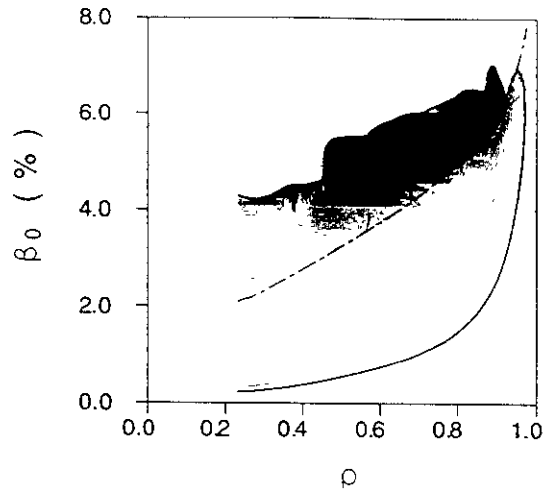
8.0
6.0
4.0
2.0
0.0
β_0 (%)
0.0
0.2
0.4
0.6
0.8
1.0
ρ

(e)

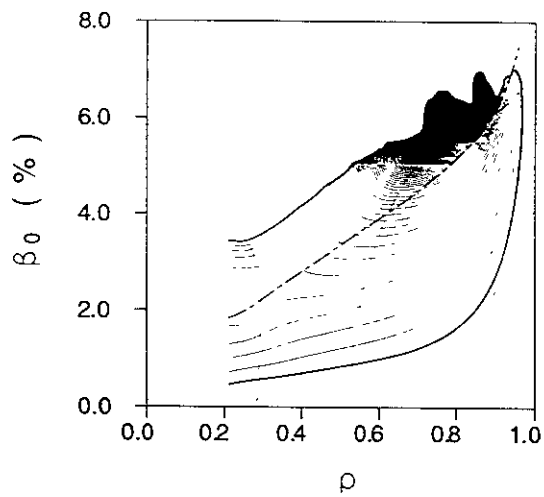
8.0
6.0
4.0
2.0
0.0
β_0 (%)
0.0
0.2
0.4
0.6
0.8
1.0
ρ

(f)

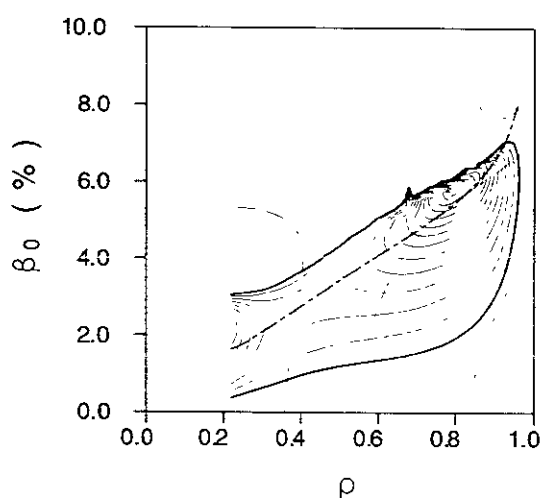
10.0
8.0
6.0
4.0
2.0
0.0
β_0 (%)
0.0
0.2
0.4
0.6
0.8
1.0
ρ

Fig.5 (d),(e),(f)

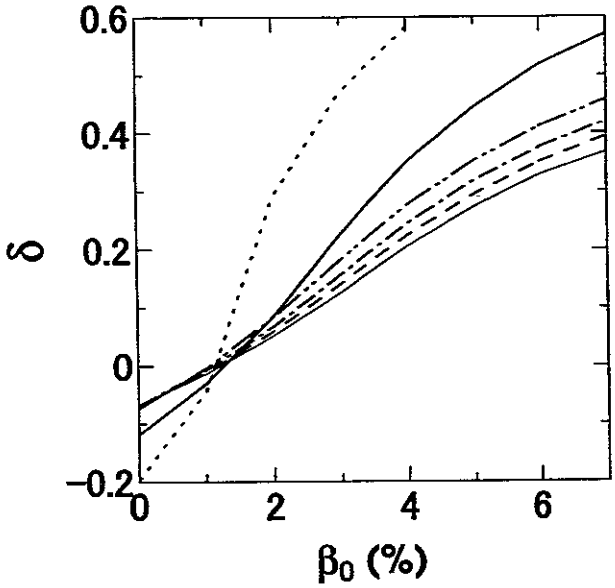

Fig.6

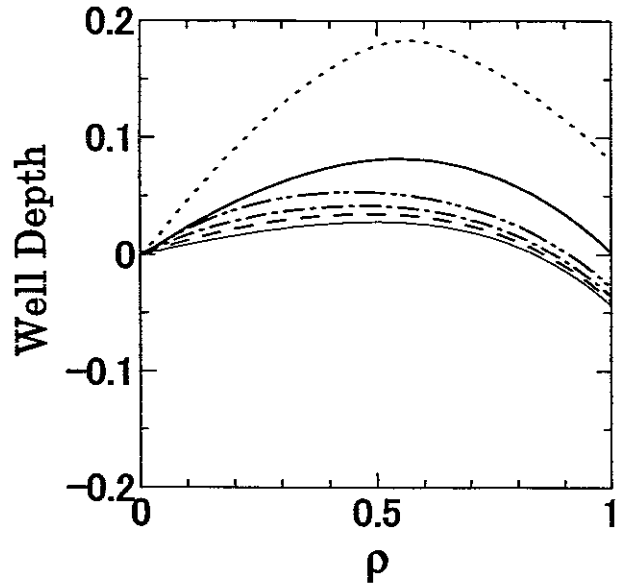

Fig.7

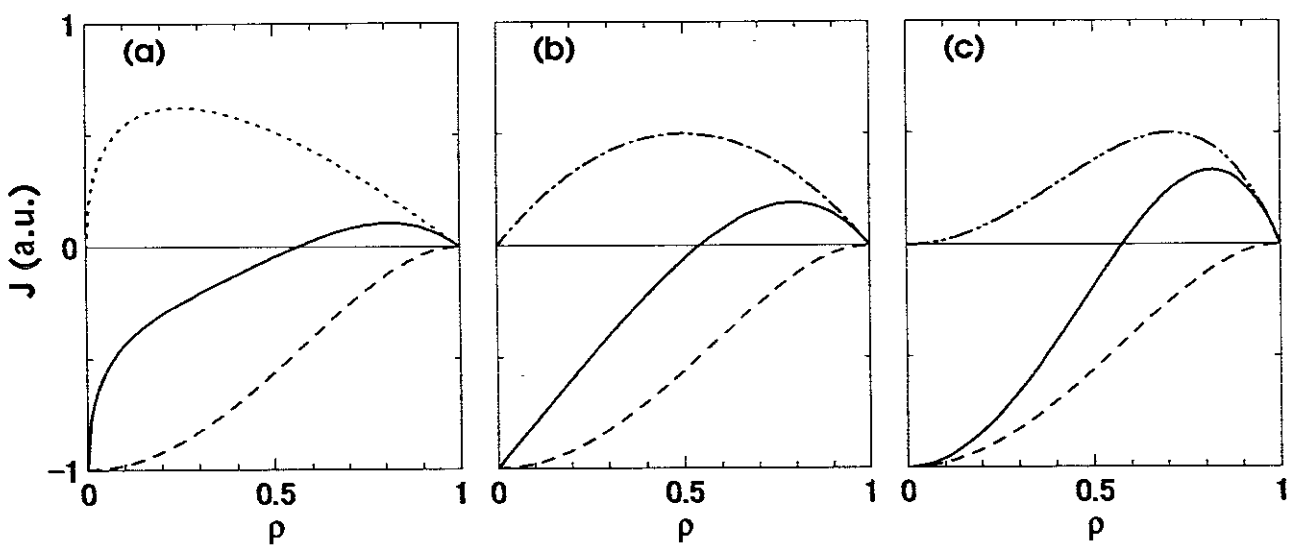

Fig.8

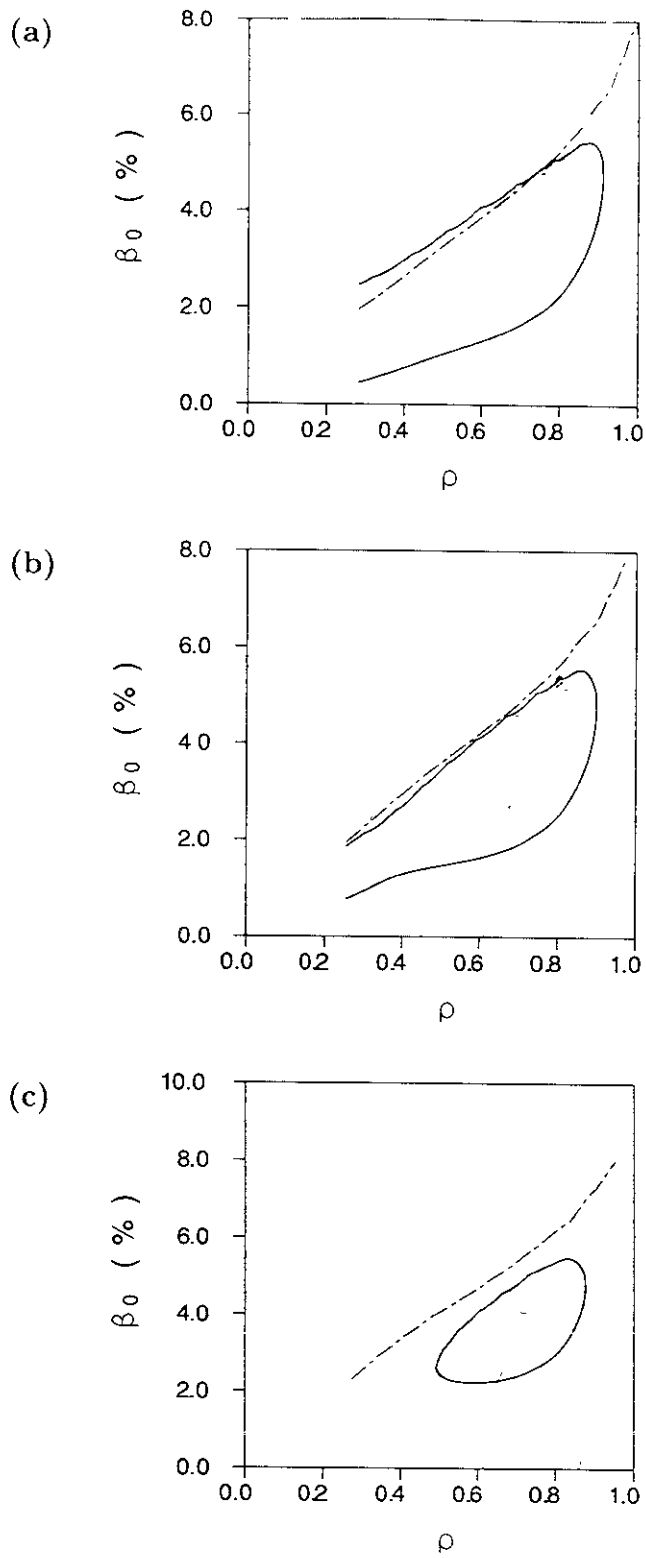
(a)
8.0
6.0
4.0
2.0
0.0
β_0 (%)
0.0
0.2
0.4
0.6
0.8
1.0
ρ
(b)
8.0
6.0
4.0
2.0
0.0
β_0 (%)
0.0
0.2
0.4
0.6
0.8
1.0
ρ
(c)
10.0
8.0
6.0
4.0
2.0
0.0
β_0 (%)
0.0
0.2
0.4
0.6
0.8
1.0
ρ

Fig.9 (a),(b),(c)

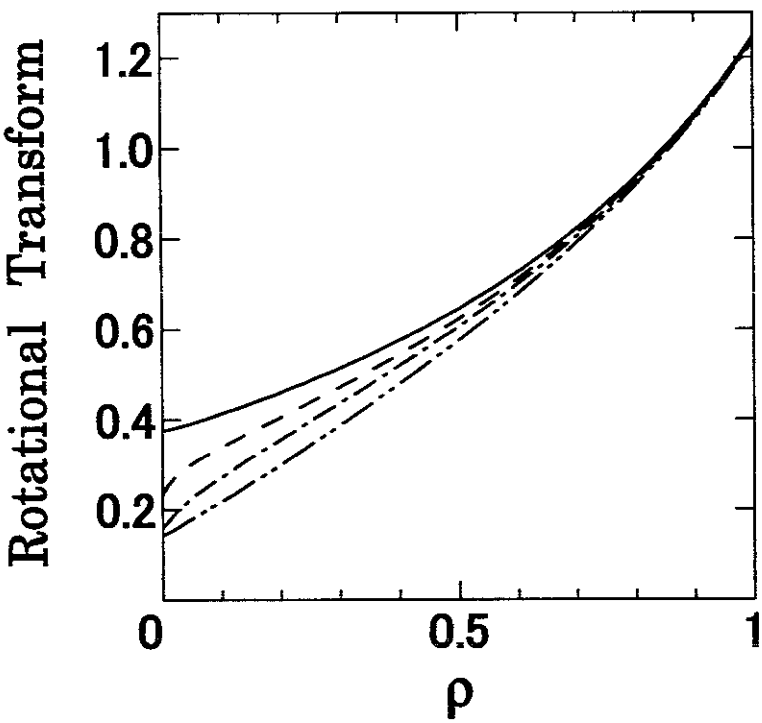

Fig.10

(a)

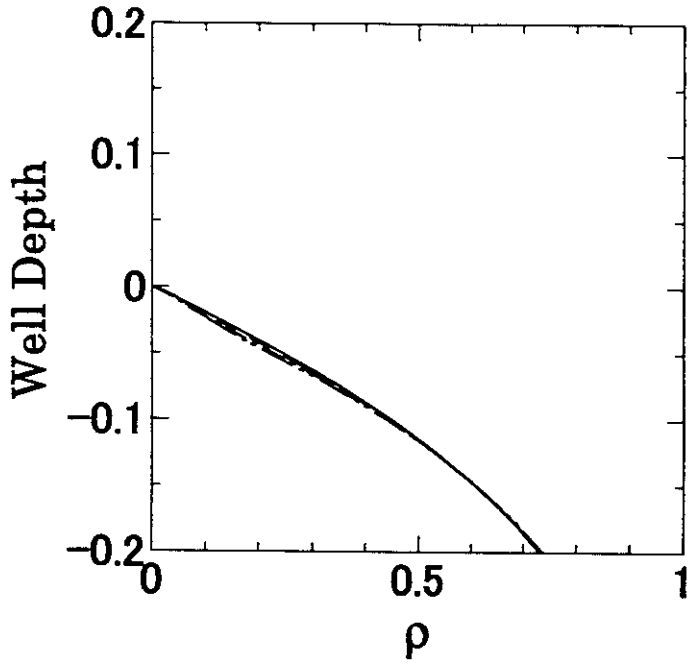

(b)

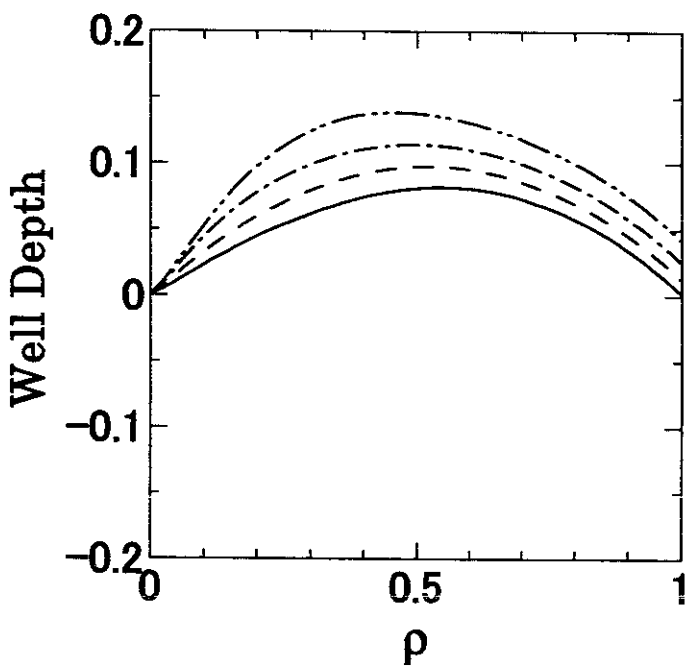

Fig.11

(a)

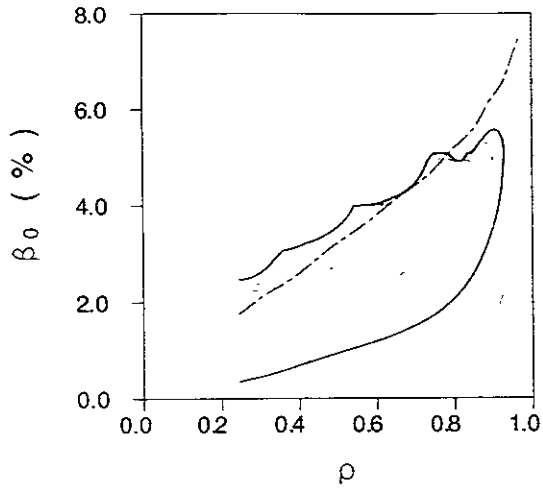

(b)

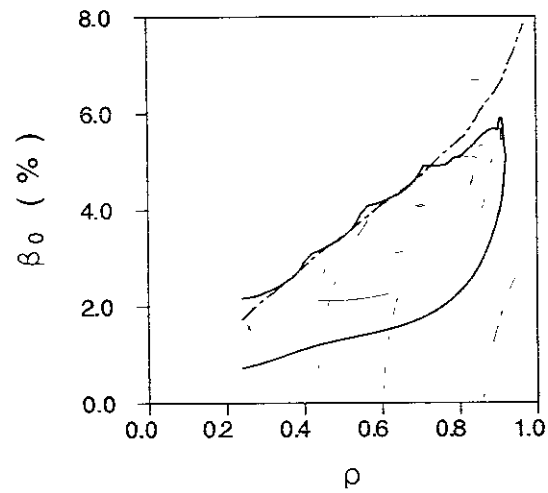

(c)

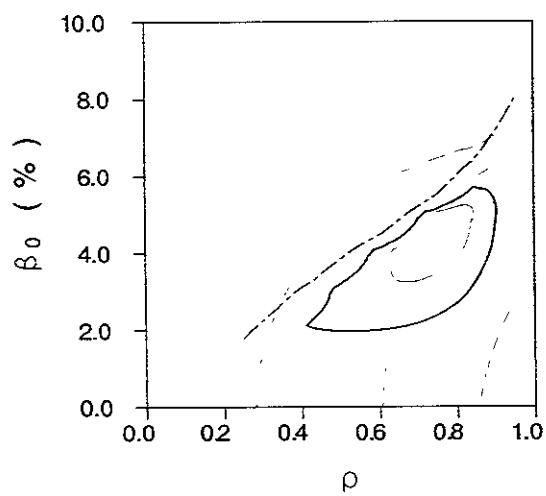

Fig.12 (a),(b),(c)

Recent Issues of NIFS Series

NIFS-668 T Mutoh, R Kumazawa, T Seki, K Saito, Y Torii, F Shimpo, G Nomura, T Watari, D A Hartmann, M Yokota, K Akaishi, N Ashikawa, P deVries, M Emoto, H Funaba, M Goto, K Ida, H Idei, K Ikeda, S Inagaki, N Inoue, M Isobe, O Kaneko, K Kawahata, A Komori, T Kobuchi, S Kubo, S Masuzaki, T Morisaki, S Morita, J Miyazawa, S Murakami, T Minami, S Muto, Y Nagayama, Y Nakamura, H Nakanishi, K Narihara, N Noda, K Nishimura, K Ohkubo, N Ohyabu, S Ohdachi, Y Oka, M Osakabe, T Ozaki, B J Peterson, A Sagara, N Sato, S Sakakibara, R Sakamoto, H Sasao, M Sasao, M Sato, T Shimozuma, M Shoji, S Sudo, H Suzuki, Y Takeiri, K Tanaka, K Toi, T Tokuzawa, K Tsumori, K Y Watanabe, T Watanabe, H Yamada, I Yamada, S Yamaguchi, K Yamazaki, M Yokoyama, Y Yoshimura, Y Hamada, O Motojima, M Fujiwara
Fast and Slow Wave Heating of Ion Cyclotron Range of Frequencies in the Large Helical Device Nov 2000

NIFS-669 K Mima, M S Jovanovic, Y Sentoku, Z-M Sheng, M M Skoric and T Sato
Stimulated Photon Cascade and Condensate in Relativistic Laser plasma Interaction Nov 2000

NIFS-670 L Hadzievski, M M Skoric and T Sato,
On Origin and Dynamics of the Discrete NLS Equation Nov 2000

NIFS-671 K Ohkubo, S Kubo, H Idei, T Shimozuma, Y Yoshimura, F Leuterer, M Sato and Y Takita
Analysis of Oversized Sliding Waveguide by Mode Matching and Multi-Mode Network Theory Dec 2000

NIFS-672 C Das, S Kida and S Goto,
Overall Self-Similar Decay of Two-Dimensional Turbulence Dec 2000

NIFS-673 L.A Bureyeva, T Kato, V.S Lisitsa and C Namba
Quasiclassical Representation of Autoionization Decay Rates in Parabolic Coordinates Dec 2000

NIFS-674 L A Bureyeva, V.S Lisitsa and C Namba,
Radiative Cascade Due to Dielectronic Recombination Dec 2000

NIFS-675 M F Heyn, S V Kasilof, W Kernbichler, K Matsuoka, V V Nemov, S Okamura, O S Pavlichenko,
Configurational Effects on Low Collision Plasma Confinement in CHS Heliotron/Torsatron, Jan 2001

NIFS-676 K Itoh,
A Prospect at 11th International Toki Conference - Plasma physics, quo vadis?, Jan 2001

NIFS-677 S Satake, H Sugama, M Okamoto and M Wakatani
Classification of Particle Orbits near the Magnetic Axis in a Tokamak by Using Constants of Motion Jan 2001

NIFS-678 M Tanaka and A Yu Grosberg
Giant Charge Inversion of a Macroion Due to Multivalent Counterions and Monovalent Coions Molecular Dynamics Studyn Jan 2001

NIFS-679 K Akaishi, M Nakasuga, H Suzuki, M Iima, N Suzuki, A Komori, O Motojima and Vacuum Engineering Group,
Simulation by a Diffusion Model for the Variation of Hydrogen Pressure with Time between Hydrogen Discharge Shots in LHD, Feb 2001

NIFS-680 A Yoshizawa, N Yokoi, S Nisizima, S -I Itoh and K Itoh
Variational Approach to a Turbulent Swirling Pipe Flow with the Aid of Helicity, Feb 2001

NIFS-681 Alexander A Shishkin
Estafette of Drift Resonances Stochasticity and Control of Particle Motion in a Toroidal Magnetic Trap, Feb. 2001

NIFS-682 H Momota and G H Miley,
Virtual Cathode in a Spherical Inertial Electrostatic Confinement Device, Feb 2001

NIFS-683 K Saito, R Kumazawa, T Mutoh, T Seki, T Watari, Y Torii, D A Hartmann, Y Zhao, A Fukuyama, F Shimpo, G Nomura, M Yokota, M Sasao, M Isobe, M Osakabe, T Ozaki, K Narihara, Y Nagayama, S Inagaki, K Itoh, S Morita, A V Krasilnikov, K Ohkubo, M Sato, S Kubo, T Shimozuma, H Idei, Y Yoshimura, O Kaneko, Y Takeiri, Y Oka, K Tsumori, K Ikeda, A Komori, H Yamada, H Funaba, K Y Watanabe, S Sakakibara, M Shoji, R Sakamoto, J Miyazawa, K Tanaka, B J Peterson, N Ashikawa, S Murakami, T Minami, S Ohakachi, S Yamamoto, S Kado, H Sasao, H Suzuki, K Kawahata, P deVries, M Emoto, H Nakanishi, T Kobuchi, N Inoue, N Ohyabu, Y Nakamura, S Masuzaki, S Muto, K Sato, T Morisaki, M Yokoyama, T Watanabe, M Goto, I Yamada, K Ida, T Tokuzawa, , N Noda, S Yamaguchi, K Akaishi, A Sagara, K Toi, K Nishimura, K Yamazaki, S Sudo, Y Hamada, O Motojima, M Fujiwara
Ion and Electron Heating in ICRF Heating Experiments on LHD Mar 2001

NIFS-684 S Kida and S Goto,
Line Statistics Stretching Rate of Passive Lines in Turbulence Mar 2001

NIFS-685 R Tanaka, T Nakamura and T Yabe,
Exactly Conservative Semi-Lagrangian Scheme (CIP-CSL) in One-Dimension Mar 2001

NIFS-686 S Toda and K Itoh,
Analysis of Structure and Transition of Radial Electric Field in Helical Systems Mar 2001

NIFS-687 T Kuroda and H Sugama,
Effects of Multiple-Helicity Fields on Ion Temperature Gradient Modes Apr 2001

NIFS-688 M Tanaka
The Origins of Electrical Resistivity in Magnetic Reconnection Studies by 2D and 3D Macro Particle Simulations Apr 2001

NIFS-689 A Maluckov, N Nakajima, M Okamoto, S Murakami and R Kanno
Statistical Properties of the Neoclassical Radial Diffusion in a Tokamak Equilibrium Apr 2001

NIFS-690 Y Matsumoto, T Nagaura, Y Itoh, S-I Itoh, K Itoh and T Watanabe
LHD Type Proton-Boron Reactor and the Control of its Peripheral Potential Structure Apr 2001

NIFS-691 A Yoshizawa, S -I Itoh, K Itoh and N Yokoi,
Turbulence Theories and Modelling of Fluids and Plasmas Apr 2001

NIFS-692 K Ichiguchi, T Nishimura, N Nakajima, M Okamoto, S -i Oikawa, M Itagaki,
Effects of Net Toroidal Current Profile on Mercier Criterion in Heliotron Plasma Apr 2001